Numerical Simulation of Surface Effects on Spinodal Decomposition in Polymer Binary Mixture: Quench Depth Dependence

ARTICLE *in* MACROMOLECULES · FEBRUARY 2006

Impact Factor: 5.8 · DOI: 10.1021/ma0524878

2 AUTHORS, INCLUDING:

Xu-Ming Xie
Tsinghua University
168 PUBLICATIONS **1,590** CITATIONS

Numerical Simulation of Surface Effects on Spinodal Decomposition in Polymer Binary Mixture: Quench Depth Dependence

Li-Tang Yan and Xu-Ming Xie*

Advanced Materials Laboratory, Department of Chemical Engineering, Tsinghua University, Beijing 100084, P. R. China

Received November 21, 2005; Revised Manuscript Received January 11, 2006

ABSTRACT: The surface-directed spinodal decomposition (SDSD) in binary polymer mixture with different quench depths is investigated by numerical simulations, combining Cahn−Hilliard−Cook (CHC) theory with Flory−Huggins−de Gennes theory. The formation mechanisms of the wetting layer with different quench depths are discussed. The simulated results demonstrate that the growth of the wetting layer can exhibit pure diffusion-limited growth law, logarithm growth law, and Lifshitz−Slyozov (LS) growth law with the increasing quench depth, which reproduces experimental observations. Furthermore, the detailed ranges of these three regimes are determined on the basis of simulated results. The growth law of the wetting layer is pure diffusion-limited growth law when $\chi N < 2.01$. In the case of $2.08 \leq \chi N$, the growth of the wetting layer obeys LS growth law. However, when $2.01 \leq \chi N < 2.08$, the logarithm growth law of the wetting layer is favored. The simulated results also demonstrate that the evolution of the polymer morphology in the parallel cross sections near the substrate surface obeys LS growth law. Moreover, the orientation effect of the surface on the dynamic behavior of these cross sections with deeper quench depth is more remarkable than that with shallower one.

1. Introduction

In the past decades, there is much considerable attention on the dynamics of phase separation via spinodal decomposition (SD) in critical binary polymer blends or other mixtures.[1,2] Almost all investigations show that the growth of domains in bulk obeys a scaling law. Deferent values of the growth exponent describe deferent mechanisms controlling the domain growth: 1/3 and 1 for LS growth without and with hydrodynamic interactions, respectively.[1−4] Theoretically, Cahn and Hilliard first propose a theory for the process of the binary metal alloys.[5] This has been extended to polymeric systems by de Gennes,[6] Pincus,[7] and Binder[8] by combination with the well-known Flory−Huggins[9] theory.

It is noted that, in the past two decades, the research attention was shifting to SD systems in thin films near the surface with different wetting abilities.[10−12] We collect the studies concerning the experimental observations of polymer mixtures in ref 10 and the works regarding the numerical simulations in ref 11.These previous studies show that the phase separation process in thin films becomes much more complex mainly because of the influences of the interactions with the surface or interface, the anisotropy of growths in various directions, and their coupling with each other. The preferential attraction of the surface is able to cause SDSD. In this case, the surface or interface is completely or partially wetted by the preferred component and becomes the origin of anisotropic SD waves which propagates into the bulk perpendicular to the surface.[10a,g−i] It has been confirmed by experimental observations[10] and numerical simulations[11] that the character length parallel to surface can grow faster than the perpendicular one in the case of SDSD. Moreover, both of them may grow in a way different from their bulk system. For example, Sung et al.[5g] found that the growth exponent of the character length parallel to surface exhibits about 1/2 in thin film samples of a polymer mixture with a 20 nm thickness. A similar scaling behavior is also observed by Hashimoto and co-workers in the biphasic region of a main-chain thermotropic liquid crystal (LC) copolyester.[5h,i] At the same time, the numerical simulations of thin film carried out by Puri et al.,[11c] Toxvaerd,[11g] and others[11i] reconfirmed this scaling behavior. It has been demonstrated that the growth exponent of the character length parallel to surface can increase from 1/3 to 1/2 at a critical time, compared to the decrease of that in the perpendicular direction.[11c,g,i] They further showed that the critical time increases with the thickness.

Currently, the formation mechanism and evolution dynamics of the wetting layer, with the effect of surface, are also taken into account. As a matter of fact, there are still many arguments for the understanding of this problem under different conditions. For instance, it has been claimed that the LS growth law would characterize the growth of the wetting layer.[13] However, the study of other authors demonstrates that this claim is valid only in the limit of partially wet morphology.[11c] Here we would like to mention an excellent work of simulations by Puri and Binder on the SDSD with off-critical initial conditions.[11d,e] Their analytical and numerical results show that the growth exponent of the wetting layer thickness can exhibit $1/(n + 1)$ (surface potential-dependent growth law), 1/3 (LS growth law), and 1/2 (pure diffusion-limited growth law[14]), where n is the exponent of the long-range surface potential. It can be observed that these different mechanisms have tight relations with the phase morphology of the wetting layer and the bulk, induced by different off-critical degrees.

As known, the quench depth can also be used to tune the morphology of the phase separation. Thus, it can be expected that the formation mechanism and evolution dynamics of the wetting layer should change with the quench depth. In fact, the corresponding experimental studies, for the polymer system, have been done.[10m,f] For instance, the experimental results of Geoghegan and co-workers demonstrated that three growth laws for the wetting layer, i.e., logarithm growth law, LS growth law, and pure diffusion-limited growth law, can be identified with different quench depths. However, the question as to what precedes the wetting layer with different quench depths is still

* Corresponding author: e-mail xxm-dce@mail.tsinghua.edu.cn; Tel +86-10-62773607; Fax +86-10-62784550.

10.1021/ma0524878 CCC: $33.50
Published on Web 02/21/2006

an open one.[12] The case that, before logarithmic growth, there may be a small region of pure diffusion-limited growth with exponent 1/2 is still uncertain. Moreover, there are yet no data on how the wetting layer is formed under certain quench depths.[12] It is difficult that these above problems are only dealt with by experiments because a huge amount of work may be needed for it. However, we think that they can be considered by the simulation methods which have yet not been concerned up to now and, accordingly, is also an issue we would like to study in this work by the numerical technique.

In this paper, the SDSD with different quench depths is investigated by numerical simulations, combining Cahn−Hilliard−Cook[5,15] (CHC) theory with Flory−Huggins−de Gennes[6,9] theory. Our main purposes are to gain insight into the formation mechanisms of the wetting layer with different quench depths and to determine more certain regimes of the quench depth based on the corresponding growth laws of the wetting layer, in the case of the critical condition. The effects of the quench depth on the dynamic behavior of the morphology, in the parallel cross sections and near the substrate surface, are also considered.

2. Model and Numerical Procedure

During this investigation, a symmetric binary system is concerned, in which both components (AB) have the same degree of polymerization, N. The hydrodynamic effect is neglected throughout as although they may play an important role in the very late stage of phase separation, the early and intermediate stages should not be affected.[19b] The dynamics and morphology evolution are described by the CHC equation for diffusive field, which can be written as[5,15]

$$\frac{\partial\phi(r,t)}{\partial t} = M\nabla^2\frac{\delta F\{\phi(r,t)\}}{\delta\phi(r,t)} + \eta(r,t) \tag{1}$$

where M is a phenomenological parameter characterizing the self-diffusion ability. $\phi(r,t)$ is the volume fraction of component A at point r at time t. $\eta(r,t)$ is the thermal noise induced by Cook[15] into the Cahn−Hilliard[5] model. The total free energy, F, is really the coupling between the surface free energy (F_s) and the bulk free energy (F_b) and can be defined as[16,17]

$$F = F_s + F_b = \int_{-\infty}^{\infty}\mathrm{d}x\int_0^{\infty}\mathrm{d}z[f_{FH}(\phi) + k(\phi)(\nabla\phi)^2] + \int_{-\infty}^{+\infty}\left(-h_1\phi - \frac{1}{2}g\phi^2\right)\mathrm{d}x \tag{2}$$

where f_{FH}, in the bulk free energy F_b, is the Flory−Huggins free energy for a homogeneous blend and is given by[9]

$$f_{FH} = \frac{\phi}{N}\ln(\phi) + \frac{(1-\phi)}{N}\ln(1-\phi) + \chi\phi(1-\phi) \tag{3}$$

The gradient term $k(\phi)$ used in this work is obtained by the random phase approximation of de Gennes for an incompressible polymer blends and can be written as

$$k(\phi) = \frac{\chi {r_0}^2}{6} + \frac{l^2}{36\phi(1-\phi)} \tag{4}$$

where r_0 gives the range of the energetic interactions[8] and l is the Kuhn statistical segment length.[6] Preliminary studies showed that the composition-independent term in eq 4 has a negligible effect on structure development, and hence all calculations presented in this paper are performed with $r_0 = 0$.[6,7,19] x and z in eq 2 are rescaled scales parallel and perpendicular to surface. In the present study, we chose z axis as the direction of the surface effect and consider only one surface located at $z = 1$. Component A is set as the preferential component of the surface. h_1 and g are two parameters which have tight relations with parameters in the Flory−Huggins lattice model.[17] In terms of the deduction of Puri et al.,[11a−e] the boundary conditions of the SDSD dynamic models based on CHC equation can be described by two partial differential equations. The first equation is defined as

$$\frac{\partial\phi(x,0,\tau)}{\partial\tau} = -h_1 - g\phi(x,0,\tau) + \gamma\left.\frac{\partial\phi(x,z,\tau)}{\partial z}\right|_{z=0} \tag{5}$$

where γ is also a parameter and h_1, g, and γ characterize the static surface diagram.[11b] It should be noted that the first two terms on the right-hand side (rhs) of eq 5 are the same as those in the surface free energy (see eq 2) while the third term, depending on γ, accounts for the energy cost of gradients in composition at the surface and was derived on the basis of the Kawasaki spin-exchange model.[18] τ is the rescaled time parameter defined later. This equation rapidly drives the concentration near the surface to its equilibrium value. A second boundary condition, $\Delta J|_{x=0} = 0$, where J, defined as $J = \nabla\delta F/\delta\phi$, is the polymer flux and is used to ensure that the flux of polymer components through the surface boundary is zero, which enforces conservation of the order parameter. By lumping together eqs 1−5 and by rescaling into a dimensionless form, the dynamic equation can be obtained as follows

$$\frac{\partial\phi(\bar{r},\tau)}{\partial\tau} = \frac{1}{2}\nabla^2\left[\frac{\chi_c}{2(\chi_f-\chi_s)}\ln\frac{\phi}{1-\phi} - \frac{2\chi}{\chi_f-\chi_s}\phi + \frac{2\phi-1}{36\phi^2(1-\phi)^2}(\nabla\phi)^2 - \frac{1}{18\phi(1-\phi)}\nabla^2\phi + \left(-h_1 - g\phi + \gamma\left.\frac{\partial\phi}{\partial z}\right|_{z=0}\right)\delta(z)\right] \tag{6}$$

where χ_c is the value of χ at the critical point of the spinodal curve and χ_f is the deepest quench. χ_s is the spinodal value of χ at $\phi = \phi_0$; i.e., $\chi_s = 1/[2N\phi_0(1-\phi_0)]$, where ϕ_0 is the initial average concentration of component A, with $\phi_0 = 0.5$ for the critical condition in the present simulation. $\bar{r}$ and τ are rescaled spatial and temporal variables, respectively, given by $\bar{r} = (|\chi_f - \chi_s|)^{1/2}r/l$ and $\tau = NM(\chi_f - \chi_s)^2t/l^2$. $\delta(x)$ is the Dirac delta function, ensuring that the surface free energy only affects $z = 0$. In essence, the surface potential used in the model is short-range[11b] because the power law potential,[11c] depending on the distance from the surface, is not included in it. It should be pointed out that a similar model is also deduced by Clarke and co-workers.[19] Equation 6 can be solved using the finite difference approach.[20] Numerically, for the sake of numerical stability and higher accuracy, the Laplacian ∇^2 is discretized on the basis of the cell dynamics scheme (CDS) proposed by Oono and Puri.[21] It is then transformed as[22]

$$\nabla^2 X \rightarrow \frac{1}{a^2}(\langle\langle X\rangle\rangle - X) \tag{7}$$

where a is the cell size. $\langle\langle X(\bar{r},\tau)\rangle\rangle$ represents the following summation of $X(\bar{r})$ for the nearest neighbors ($\bar{r}.$) and the next-nearest neighbors ($\bar{r}.\bar{r}.$):

$$\langle\langle X(\bar{r})\rangle\rangle = B_1\sum_{\bar{r}=\bar{r}.}X(\bar{r}) + B_2\sum_{\bar{r}=\bar{r}.\bar{r}.}X(\bar{r}) \tag{8}$$

where B_1 and B_2 are 1/6 and 1/12, respectively. To avoid the

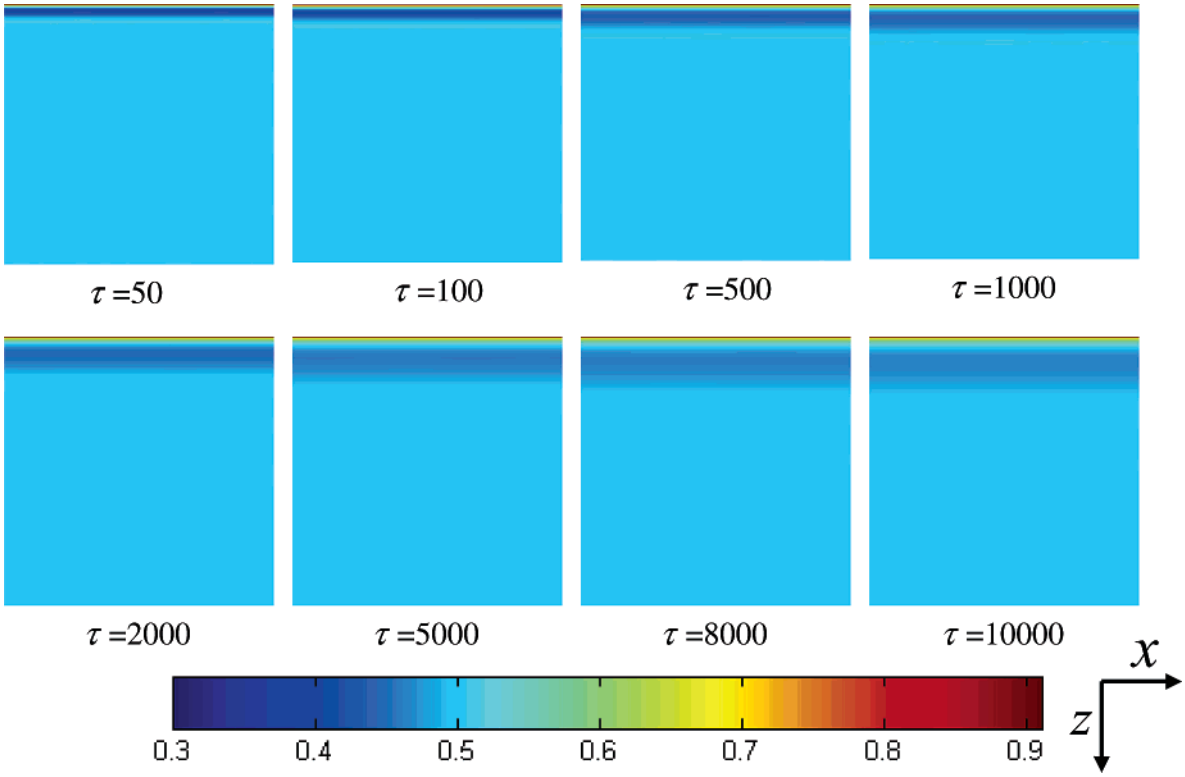

Figure 1. Development of the polymer morphology following a quench depth with $\epsilon = 0.0001$. The color bar indicates the concentration of the wetting component (A) for the surface.

discretization effect due to the lattice size,[19c] the surface terms h_1, g, and γ are rescaled by the step length of the spatial discretization, $\Delta\bar{r}$, and are listed as follows:

$$h_1 \rightarrow h_1/\Delta\bar{r}; \quad g \rightarrow g/\Delta\bar{r}; \quad \gamma \rightarrow \gamma/\Delta\bar{r} \tag{9}$$

Our simulations were carried out on a 300 × 300 two-dimensional lattice. Flat boundary conditions[11c,e] were applied at the other end in the perpendicular direction, and periodic boundary conditions were applied in the parallel direction. Noise, with the magnitude of $\pm 1 \times 10^{-3}$, was only added once at the start of the quench. $\chi_c = \chi_s = 0.01$, $h_1 = -1.5$, $g = 0.1$, $\gamma = 0.1$, and $N = 200$ were set in all simulations. To keep the length scaling of the system consistent, χ_f was fixed at 0.0133 throughout simulations. The Δt (time step) value used during the temporal discretization was 1×10^{-4}, and the spatial discretization step was $\Delta\bar{r} = 0.5$.

3. Results

3.1. Formation and Evolution of the Polymer Morphology. At first, the development of the polymer morphology in SDSD is demonstrated with the increasing quench depth. ϵ, which is defined as $\epsilon = (\chi - \chi_c)/\chi_c$, denotes the quench depth in this work. A higher ϵ corresponds to a deeper quench depth.

(A) Case of the Shallowest Quench Depth. First, the polymer morphology in SDSD with the shallowest quench depths is examined. In Figure 1, the evolution of the polymer morphology with $\epsilon = 0.0001$ is illustrated. In this case, χ is very approximate to χ_c. The concentration of component A is marked with the color bar. From Figure 1 it can be seen that the wetting layer, with A-rich phase, immediately comes into being, followed by B-rich layer or the depletion layer of component A. However, the bulk does not undergo any phase separation. In other words, the thermodynamic instability of the system is not strong enough to drive the phase separation within the time scale of our simulation. Nevertheless, the wetting layer near the surface grows rapidly. One can find that the interfaces of the wetting layer, at different times, are always flat. The features of the polymer morphology, when ϵ is smaller than 0.005, are almost the same as those in Figure 1 though they have not been exhibited here.

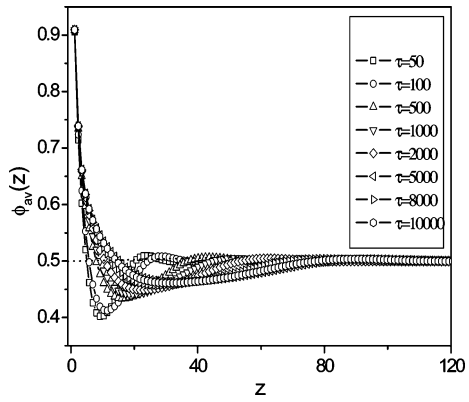

Figure 2. Averaged concentration profiles in z direction for the patterns in Figure 1 at different times.

Figure 2 shows the averaged concentration profiles in the z direction, accompanying the evolution of the polymer morphology in Figure 1. The averaged profiles are obtained by averaging the concentration profile $\phi(x,z,\tau)$ of the parallel cross sections along z axis as eq 10, with $N_x = \phi_{av}(x,0,\tau)$, for a single run and then ensemble averaging over 50 different runs.

$$\phi_{av}(z,\tau) = \frac{1}{N_x}\sum_x \phi(x,z,\tau) \tag{10}$$

Notice that the A-rich wetting layer is followed by a layer which is moderately depleted in A and extends deep into the bulk. Clearly, the averaged concentration ϕ_{av}, with the value of about

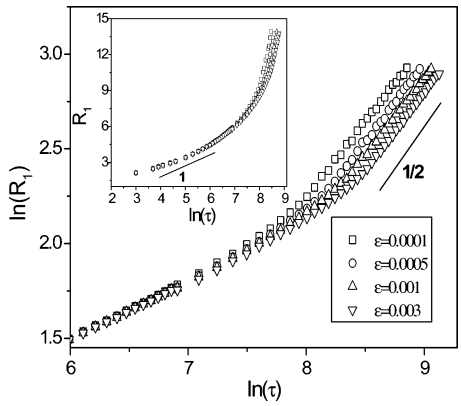

Figure 3. Log−log plots of the wetting layer thickness, R_1, vs time τ with different values of ϵ. The inset shows the corresponding plots in a single-logarithmic time scale.

0.5, is almost unchangeable in the bulk, demonstrating again that no phase separation occurs in it. It can also be found that the depth of the depletion layer becomes shallower with the increasing time.

The thickness of the surface layer, R_1, can be measured by finding the z position of the first value of 0.5 in the z-averaged concentration profile. Figure 3 illustrates the temporal evolution of R_1 in the log−log scale with different values of ϵ. The inset indicates the corresponding data in a single-logarithmic time scale. It is found that these plots cross over to a faster growth at different times in the later stage. The linear fitting plots clarify the crossover behavior. Before the crossover, the growth law is $R_1(\tau) \propto \ln \tau$ (see inset in Figure 3), demonstrating the typical logarithm growth law.[11b,f] After the crossover, the accelerated growth seems to fit a faster law with about $R_1(\tau) \propto \tau^{1/2}$, i.e., the pure diffusion-limited growth law.[14] Moreover, the larger the values of ϵ, the later the crossover is.

(B) Case of the Shallower Quench Depth. Here, we will now concentrate our attention on the polymer morphology in SDSD with shallower quench depths. Figure 4 shows the temporal evolution of the polymer morphology in SDSD with different values of ϵ, following shallower quench depths. From Figure 4A, it can be seen that the phase separation has yet not occurred in the bulk at the earlier stage when the value of ϵ increases to 0.005. However, compared to Figure 1, the feature of the two-phase separation can be identified at the later stage. However, the contrast between two phases is unclear, indicating that the extent of the phase separation is very low. One can also note that the interfaces of the wetting layer are still flat.

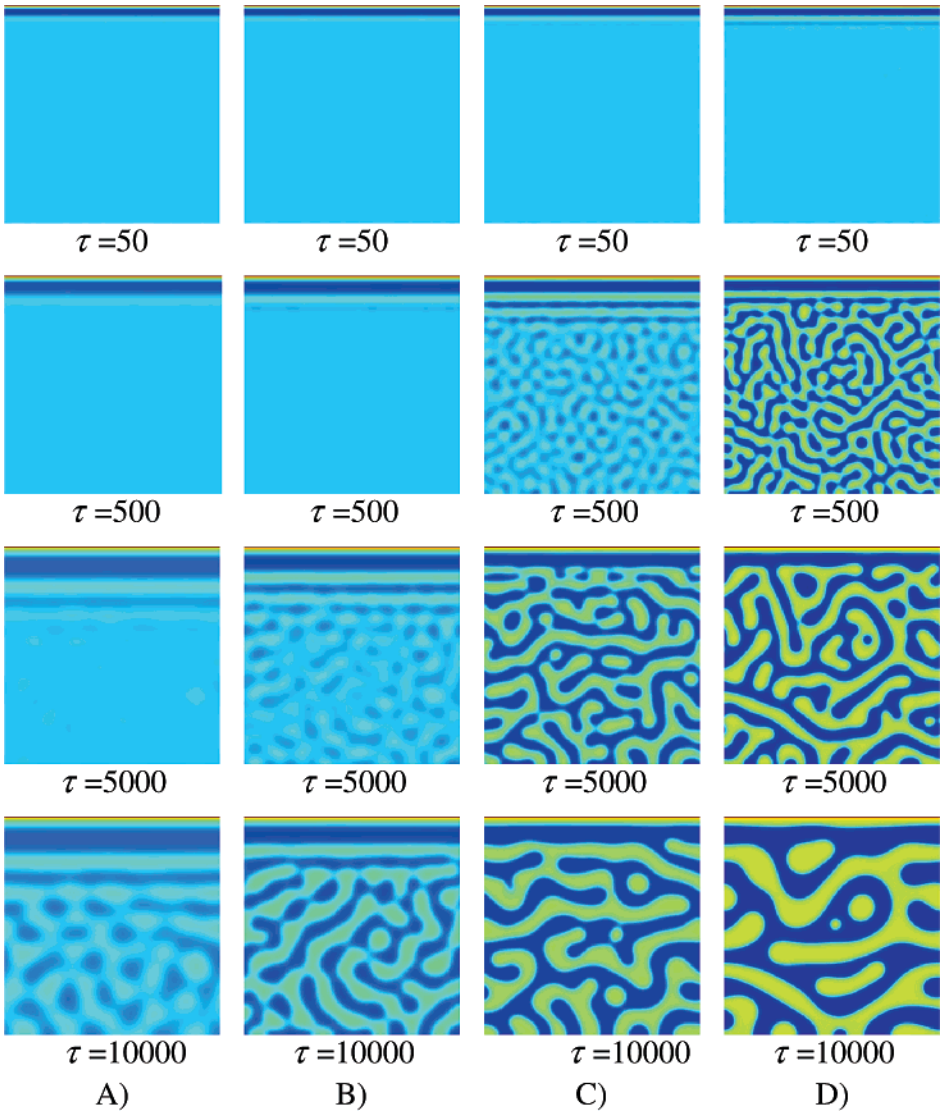

Figure 4. Development of the polymer morphology with different values of ϵ, following shallower quench depths. The color bar and the coordination are the same as those of Figure 1. (A) $\epsilon = 0.005$, (B) $\epsilon = 0.01$, (C) $\epsilon = 0.02$, and (D) $\epsilon = 0.03$.

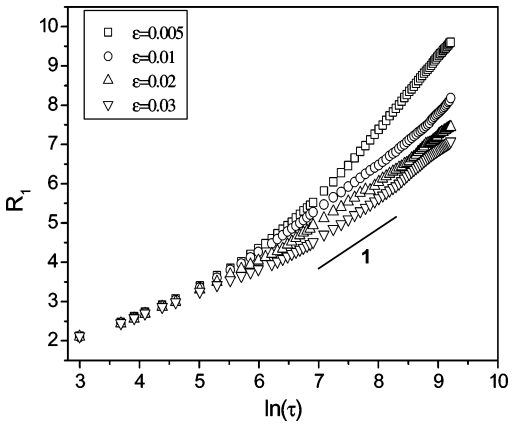

Figure 5. Single-logarithmic plots of the wetting layer thickness, R_1, vs time τ with different values of ϵ.

With the increasingϵ, the same change of polymer morphology can be observed until $\epsilon = 0.03$, although the bulk begins to undergo phase separation at earlier stage for a larger ϵ, and the contrast between two phases becomes obvious. It is worth to note that the interface of the wetting layer, in Figure 4D, begins to fluctuate mildly at a later stage of the phase separation.

The temporal evolution of the wetting layer, R_1, corresponding to Figure 4 is shown in Figure 5 in a single-logarithmic time scale. It can be found that the values of R_1 with lower ϵ are considerably larger than those with higher one, demonstrating, to a certain extent that the growth of the wetting layer is directed by the substrate surface potential. The curves of R_1 with different values of ϵ cross over to the logarithm growth law at the later stage. Moreover, a higher value of ϵ corresponds to an earlier crossover. One can find that the growth of the wetting layer with $\epsilon = 0.03$ favors a faster growth in the much later stage, corresponding to the observation in Figure 4. It should be pointed out that the growth behavior of the wetting layer in the earliest stage will not be considered because the thermal noise affects it much more, and it is too short to be measured in the experiment.

(C) Case of the Deepest Quench Depth. Finally, we consider the evolution of the polymer morphology with deep quench depths. The typical development of the polymer morphology with deep quench depths is illustrated by the images in Figure 6. It is obvious that the bulk immediately begins to undergo phase separation at the earlier stage when the value of ϵ increases to be 0.04 or larger values. Because of symmetry, the structures exhibit the characteristic cocontinuous morphology. A deeper

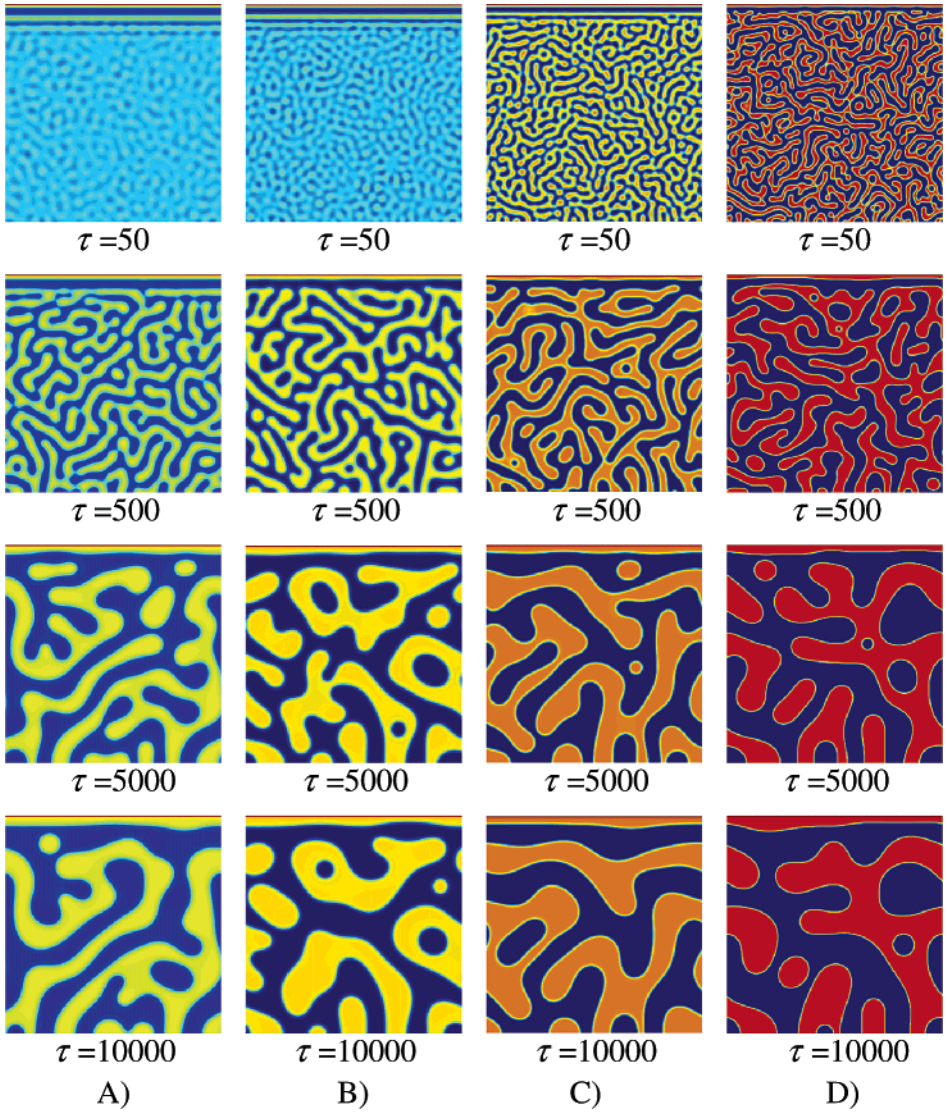

Figure 6. Development of the polymer morphology with different values of ϵ, following deep quench depths. The color bar and the coordination are the same as those of Figure 1. (A) $\epsilon = 0.04$, (B) $\epsilon = 0.06$, (C) $\epsilon = 0.12$, and (D) $\epsilon = 0.175$.

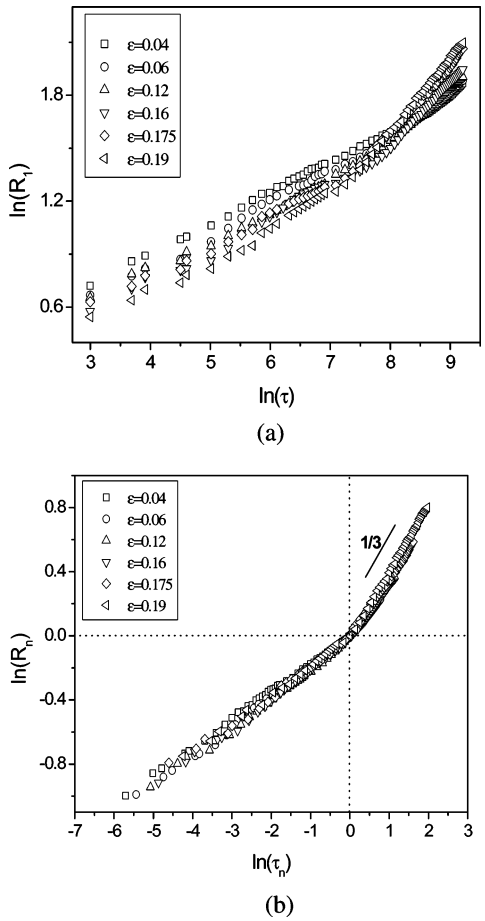

Figure 7. (a) Log−log plots of the wetting layer thickness, R_1, vs time τ with different values of ϵ. (b) Log−log plots of the reduced wetting layer thickness, R_n, against time, τ_n.

quench depth corresponds to a higher extent of phase separation. The composition fractions of AB components reach an equilibrium state quickly in the bulk. Our simulations demonstrate that the percolated network in the bulk becomes very unstable, so it gradually disrupts or breaks into many fragments. With further increasing time, the irregularly shaped anisotropic fragments shrink and then reshape into many anisotropic drops or droplets, corresponding to the experimental observations.[10h,i] It can be seen that the fluctuation of the wetting layer interface occurs at earlier stage and is more considerable than those with shallower quench depths.

The double-logarithmic plots of R_1 vs τ in Figure 7, with the same quench depths as those in Figure 6, show the quench depth effect on the evolution of the wetting layer with deep quench depths. From Figure 7a, one can see that, for the six quench depths selected, the growths of the wetting layer thickness can cross over to faster growths. One can see that a deeper quench depth can lead to an earlier crossover which is followed by a faster growth. Clearly, the values of R_1, at the fixed time before the crossover of $\epsilon = 0.19$, decrease when the quench depth parameter, ϵ, rises from 0.04 to 0.19. It can also be found from Figure 7a that, compared to the regime of the shallower quench depth, i.e., Figure 5, the differences among the critical times of the crossovers with different values of ϵ are more considerable. Moreover, the differences of the values of R_1, with different quench depths, are very small. Thus, the wetting layer thickness with higher values of ϵ can exceed those with lower ones in the much later stage.

In Figure 7a, it is found that the six straight lines are parallel after the crossover. To determine the growth law of the wetting layer in the later stage, a master curve may be obtained if we properly shift all these curves along log τ and log R_1 axes. At first, the R_1 and τ at the crossover of these curves, denoted as R_c and τ_c, respectively, are defined. Then, the scaled wetting layer thickness and the scaled time can be written as follows:

$$R_n = \frac{R_1}{R_c}, \quad \tau_n = \frac{\tau}{\tau_c} \tag{11}$$

Clearly, R_c and τ_c are functions of the quench depth. Figure 7b illustrates the plots of R_n vs τ_n in a log−log scale. The curves, with different quench depths, fall on a master curve after the crossovers, demonstrating that the wetting layers, at this regime, grow with the same growth law. The solid line in the figure indicates that the growth of the wetting layers after crossovers obeys the scaling law $R_n(\tau) \propto \tau^{1/3}$, which implies that, with the deep quench depths or $\epsilon \geq 0.04$, the growth law of the wetting layers is the typical LS growth law.

3.2. Dynamic Behavior in the Parallel Cross Sections near the Substrate Surface. The polymer morphologies, at the same time $\tau = 1000$ and following different quench depths, are collected and listed in Figure 8. This demonstrates that a deeper quench depth leads to a higher extent of phase separation and a more extreme fluctuation of the wetting layer interface, corresponding to our above simulation results. It can also be found that the phase structure, in the cross sections near the substrate surface and following the depletion layer, will orientate along the parallel direction, which has been reported in the experimental observations[10g−i] and other simulation works.[11c,d,f,i] The preferential attraction of the substrate surface can accelerate the growth of the character length parallel to the substrate surface, compared to suppressing that perpendicular to the substrate surface. Thus, the dynamic behavior of the polymer morphology is relatively changed. In this section, our concentration turns to this orientation effect with different quench depths.

The scaling behavior of real-space correlation functions, which are useful in characterizing the dynamics of fluctuations, are induced to gain insight into the effects of the substrate surface on the dynamic behavior near the substrate surface. The z-dependent correlation function perpendicular to the substrate can be defined as[11b,c]

$$G(z_1,z,\tau) = \langle \phi(x,z,\tau)\, \phi(x,z+z_1,\tau)\rangle - \langle \phi(x,z,\tau)\rangle\langle \phi(x,z+z_1,\tau)\rangle \tag{12}$$

The angular brackets refer to an averaging over initial conditions and integration over x. Figure 9 is the temporal evolution of the laterally averaged correlation function, $G(z_1,z,\tau)$, as a function of z_1 for $z = 20$ and $\epsilon = 0.1$. It is obvious that the fluctuation scope increases with the increasing time, corresponding to the change of the extent of the phase separation.

Furthermore, the characteristic length in the perpendicular direction, L, can be defined as

$$G(z+L,z,\tau) = G(0,z,\tau)/2 \tag{13}$$

where $G(0,z,\tau)$ is the maximum value of $G(z_1,z,\tau)$. Figure 10 plots L against time τ for $\epsilon = 0.06$, 0.1, 0.16, and 0.19 at $z = 20$. All plots are calculated with a single run and then ensemble averaging over 50 different runs. For simplicity, we only consider the polymer morphology with deep quench depths. It is found that L exhibits power-law growth, i.e., $L(\tau) \propto \tau^{\alpha}$, from the interim to the later stages. The scaling exponent, α, with different quench depths can be obtained by linear fitting and is indicated in the inset of Figure 10. One can see that all these

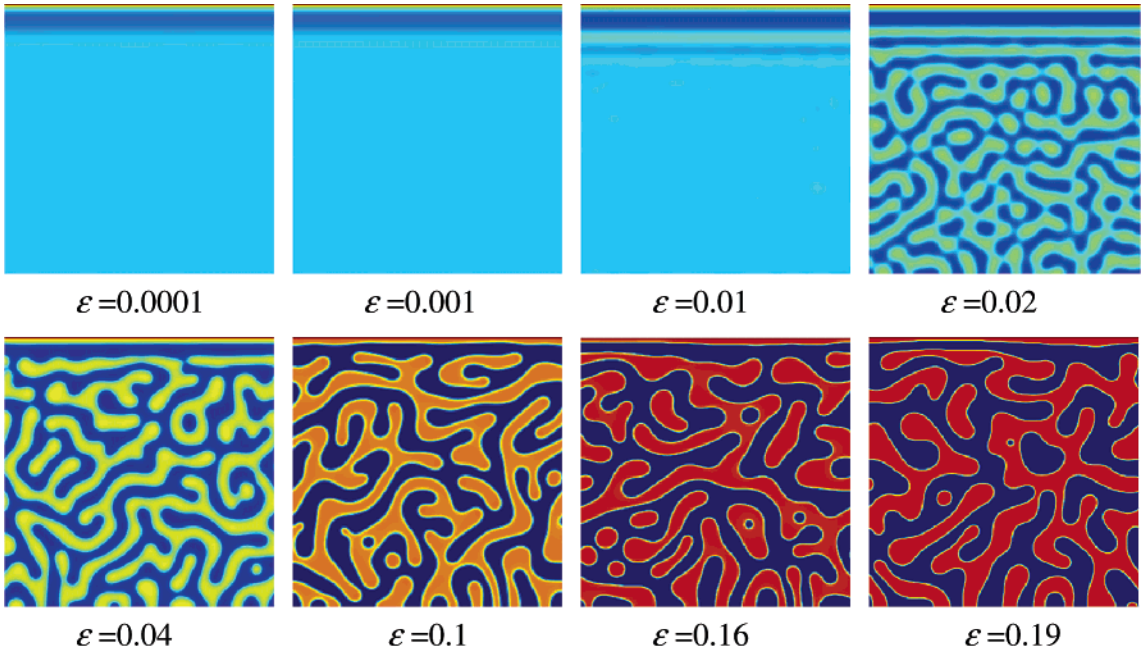

Figure 8. Polymer morphology following different quench depths, ϵ, at the same time, $\tau = 1000$. The color bar and the coordination are the same as those of Figure 1.

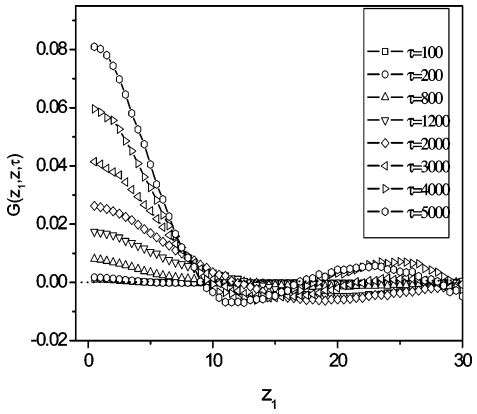

Figure 9. Laterally averaged correlation function, $G(z_1,z,\tau)$, as a function of z_1 for $z = 20$ and $\epsilon = 0.1$.

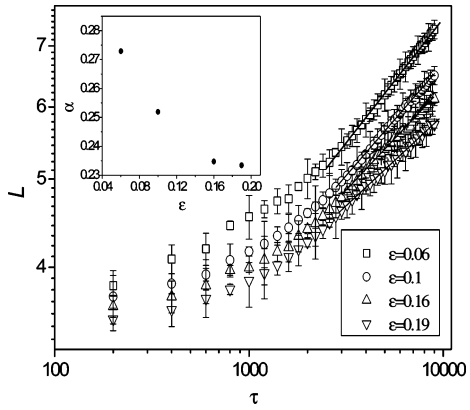

Figure 10. Plots of L against time τ at $z = 20$ with different values of ϵ. The inset indicates the change of the growth exponents, α, vs ϵ.

growth exponents with different quench depths approximate to 1/3, demonstrating that the evolution of the polymer morphology, in the parallel cross sections and near the substrate surface, still obeys LS growth law. Moreover, the inset of Figure 10 illustrates that a shallower quench depth corresponds to a higher value of the scaling exponent, which implies that the orientation effect of the surface on the dynamic behavior of the parallel cross sections with deeper quench depth is more remarkable than that with the shallower one.

4. Discussion

4.1. Formation Mechanism of the Wetting Layer. The formation mechanism of the wetting layer is our major concern in this work. As briefly emphasized in section 3, the growth low of the wetting layer has a tight relation with the polymer morphology driven by different quench depths. Moreover, it is obvious from Figures 1, 4, and 6 that the polymer morphology can be tuned by alternating the quench depth, leading to different formation mechanisms of the wetting layer. Basically, in terms of the growth law of the wetting layer, the quench depth can be divided into three regimes which will be discussed in detail in this section.

Our simulation demonstrates that there does be a regime with exponent 1/2 for the evolution of the wetting layer before the appearance of the logarithm growth law, which proves the assumption of Geoghegan et al.[10f] based on the experimental observation. It locates in the shallowest quench depth regime or $\epsilon < 0.05$. In this case, there is no phase separation in the bulk at both early and late stages. The bulk is behaving like a semiinfinite reservoir for the wetting layer. Thus, the growth law of the wetting layer is the pure diffusion-limited growth law ($\tau^{1/2}$).[14]

Our simulation also indicates that there does be a regime with the logarithm growth law of the wetting layer in the shallower quench depth. The simulation indicates that the range of ϵ corresponding to this regime is about $0.05 \leq \epsilon < 0.4$. In the regime, the bulk begins to undergo phase separation although its extent is very shallow. As the evolution of this phase separation structure, there is less material to be supplied to the wetting layer, leading to a slower growth rate. So, the wetting layer cannot grow with a pure diffusion-limited $\tau^{1/2}$ growth; instead, it grows logarithmically with time.

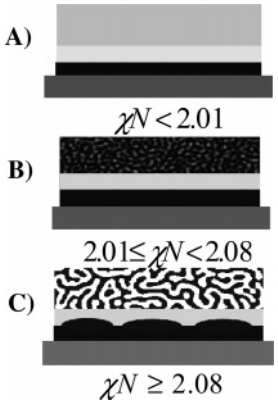

Figure 11. Schematic diagrams illustrating the regimes of the growth law for the wetting layer: (A) pure diffusion-limited growth law; (B) logarithm growth law; C) Lifshitz −Slyozov growth law.

When the value of ϵ is equal to 0.4, even larger than it, the wetting layer is not stable, and droplets are formed near the surface. The wetting layer is no longer stable because the value of ϵ is so larger that a growing flat wetting layer interface cannot survive and breaks up. Here, there is also phase separation in the bulk, and both the wetting layer and bulk droplets are growing with $\tau^{1/3}$ behavior because they are both exhibiting LS growth law. The simulation reproduces the experimental results.[10f]

However, it should be noted that those values of ϵ used in the experiment of Geophehagan et al.[10f] do not belong to their corresponding regimes determined in our simulation. This is due to the fact that the parameters ϵ and χ have tight relations with the degree of the polymerization, N.[1] For the convenience of understanding, these regimes are calculated and divided again on the basis of the parameter χN. Figure 11 is the schematic diagram representing these three regimes with the parameter χN.

It has been demonstrated theoretically[24] and experimentally[10f] that when there is only one relevant length scale present, or when all length scales have the same growth law, dynamic scaling should occur. Thus, the dynamic scaling can be used to test our conclusion about the growth laws in different regimes. Figure 12 shows the dynamic scaling results in each of the growth regimes. In the regime of the shallowest quench depth, there is no phase separation in the bulk; then, dynamic scaling should occur as there is only one length scale present in the system, i.e., the thickness of the wetting layer. In the shallower quench depth regime, the wetting layer is growing logarithmically, but LS coarsening is expected to be occurring in the bulk; thus, the dynamic scaling should fail in this regime. Finally, in the regime of the deepest quench depth, the wetting layer and bulk phase separation both occur with a LS behavior; thus, the dynamic scaling should be exhibited. As can be seen from Figure 12, this is indeed our conclusion about three regimes of the wetting layer.

4.2. Theory Analysis for the Mechanism of the Wetting Layer. Next we will theoretically analyze the growth laws in these three regimes on the basis of the chemical potential gradient or the current equation.[1,11d,e]

The wetting layer grows mainly due to two contributions to the chemical potential gradient (or current): the surface potential gradient, μ_s, and the difference between the intrinsic chemical potential and the flat wetting layer interface, μ_b/h, where μ_b is the chemical potential in the bulk and h is the thickness of the depletion layer. μ_s leads to the formation and growth of the wetting layer. On the contrast, the effect of μ_b/h can disturb

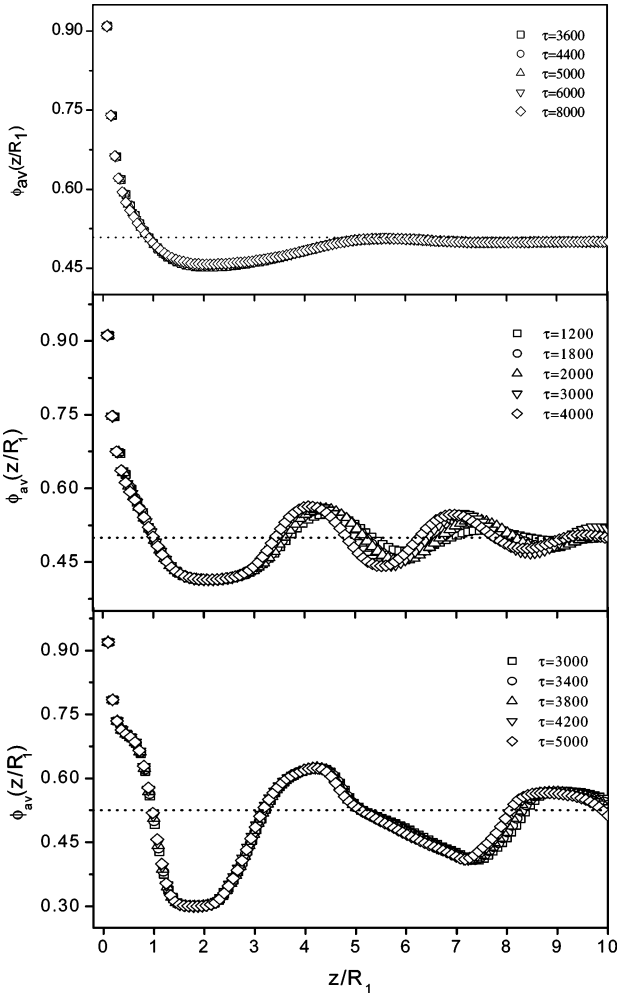

Figure 12. Dynamic scaling results in each of the growth regimes: (top) shallowest quench depth ($\epsilon = 0.0001$); (middle) shallower quench depth ($\epsilon = 0.01$); (bottom) deepest quench depth ($\epsilon = 0.06$).

and thin the wetting layer. Thus, the total chemical potential gradient, μ_t, can be described as

$$\mu_t = \frac{dR_1}{d\tau} = \mu_s - \frac{\mu_b}{h} \tag{14}$$

The surface potential $V(z)$ used in the simulation is the short-range surface potential, with $V(z) = h_1 \exp(-z/\xi)$, where ξ is the characteristic decay length.[11b,d,e] Thus, for all the simulations

$$\mu_s = \frac{dV(z)}{dz}\Big|_{z=R_1} = -\frac{h_1}{\xi}\exp\left(-\frac{R_1}{\xi}\right) \tag{15}$$

However, the detailed forms of μ_b/h in different regimes are different because the polymer morphology in the bulk will change, which has been discussed in detail by Puri and Binder.[11d,e] Our following discussions are based on their results.

(1) The deepest quench depth ($2.08 \le \chi N$). In this case, the phase separation occurs in the bulk simultaneously at the early stage and has enough strength to affect the formation of the wetting layer. Then, the μ_b/h can be defined as[11d,e]

$$\frac{\mu_b}{h} = \frac{\sigma}{R_0 R_1}\left(\frac{1+\phi_0}{1-\phi_0}\right) \tag{16}$$

where R_0 is the character length of the phase structure in the bulk and σ is the surface tension. Thus, the form of eq 14 is

transformed as follows

$$\frac{dR_1}{d\tau} = -\frac{h_1}{\xi}\exp\left(-\frac{R_1}{\xi}\right) + \frac{\sigma}{R_0 R_1}\left(\frac{1+\phi_0}{1-\phi_0}\right) \tag{17}$$

The bulk length scale obeys the LS growth law, i.e., $R_0(\tau) = f(\bar{\psi})(\sigma\tau)^{1/3}$, where $\bar{\psi}$ is the averaged order parameter ψ with $\psi = \phi_A - \phi_B$, and the function $f(\bar{\psi})$ is known analytically in the limit $|\bar{\psi}| \to 1$.[1] As R_1 grows with time, the first term on the rhs of eq 17 is dominant at early stage and the second term is dominant at late stage. This yields the growth regimes as

$$R_1(\tau) \approx \begin{cases} \xi \ln(h_1\tau/\xi^2), & \tau \le \tau_c \\ \sqrt{\dfrac{3}{f(\bar{\psi})}\dfrac{(1+\bar{\psi})}{(1-\bar{\psi})}}(\sigma\tau)^{1/3}, & \tau \ge \tau_c \end{cases} \tag{18}$$

where τ_c is the critical crossover time and can be obtained by equating the early-time and late-time scales. Clearly, the growth low of the wetting layer in the later stage is LS growth law with a growth exponent, 1/3.

(2) The shallower quench depth ($2.01 \le \chi N < 2.08$). In this case, the bulk begins to undergo phase separation. However, the extent of the phase separation is very low, and the difference between two phases is small. Accordingly, the character length of the bulk can be assumed to be very large. Then the second term in the rhs of eq 17 can be ignored correspondingly. Thus, the growth of the wetting layer always obeys the time scaling as follows:

$$R_1(\tau) \propto \ln \xi(h_1\tau/\xi^2) \tag{19}$$

It is obvious the growth law in this regime is the logarithm growth law.

(3) The shallowest quench depth ($\chi N < 2.01$): In this case, there is no phase separation in the bulk. Thus, the μ_b/h can be defined as[11d,e,23]

$$\frac{\mu_b}{h} = \frac{|\phi_0|(1+\phi_0)B_0}{R_1} \tag{20}$$

where B_0 is a constant. Thus, eq 14 can be modified as

$$\frac{dR_1}{d\tau} = -\frac{h_1}{\xi}\exp\left(-\frac{R_1}{\xi}\right) + \frac{|\phi_0|(1+\phi_0)B_0}{R_1} \tag{21}$$

The corresponding growth laws in this case are

$$R_1(\tau) = \begin{cases} [2|\phi_0|(1+\phi_0)B_0]^{1/2}\tau^{1/2} & \tau \ge \tau_c \\ \xi \ln(h_1\tau/\xi^2) & \tau \le \tau_c \end{cases} \tag{22}$$

Therefore, there is a crossover from logarithm growth law to pure diffusion-limited growth law with growth exponent 1/2.

5. Conclusions

In this paper, the SDSD in polymer binary mixture with different quench depths is investigated by numerical simulations, combining Cahn−Hilliard−Cook theory with Flory−Huggins−de Gennes theory. Our simulated results demonstrate that the formation mechanism and evolution dynamics of the wetting layer have a tight relation with the quench depth because the polymer morphology can be tuned effectively by altering the quench depth. This reproduces the experimental observations.

The simulated results prove that there does be a regime with exponent 1/2 (pure diffusion-limited growth law) for the evolution of the wetting layer before the appearance of the logarithm growth law. The logarithm growth law occurs with a deeper quench depth when the extent of phase separation is much shallower. However, the deepest quench depth indicates the LS growth law of the wetting layer because, in this case, a growing flat wetting layer interface cannot survive and breaks up. Moreover, the detailed ranges of these three regimes are determined on the basis of our simulated results. The growth law of the wetting layer is pure diffusion-limited law when $\chi N < 2.01$. In the case of $2.08 \le \chi N$, the growth of the wetting layer obeys LS growth law. However, when $2.01 \le \chi N < 2.08$, the logarithm growth law of the wetting layer is favored.

The simulated results also demonstrate that the growth law of the polymer morphology in the parallel cross sections near the substrate surface is still LS growth law. The orientation effect of the substrate surface on the dynamic behavior of these cross sections with deeper quench depth is more remarkable than that with the shallower one.

References and Notes

(1) (a) Bray, A. J. *Adv. Phys.* **1994**, *43*, 357. (b) Furukawa, H. *Adv. Phys.* **1983**, *34*, 703. (c) Gunton, J. D.; Miguel, M. S.; Sahni, P. S. In *Phase Transition and Critical Phenomena*; Domb, C., Lebowitz, J. L., Eds.; Academic: New York, 1983; Vol. 8.

(2) (a) Hashimoto, T. *Phase Transitions* **1988**, *12*, 47. (b) In *Dynamics and Patterns in Complex Fluids*; Onuki, A., Kawasaki, K., Eds.; Springer: Berlin, 1990. (c) Hashimoto, T. In *Materials Science and Technology*; Cahn, R. W., Haasen, P., Kramer, E. J., Eds.; VCH: Weinheim, 1993; Vol. 12, Chapter 6.

(3) Lifshitz, I. M.; Slyozov, V. V. *Phys. Chem. Solids* **1961**, *19*, 35.

(4) Siggia, E. D. *Phys. Rev. A* **1979**, *20*, 595.

(5) Cahn, J. W.; Hilliard, J. E. *J. Chem. Phys.* **1958**, *28*, 258.

(6) (a) de Gennes, P. G. *Scaling Concepts in Polymer Physics*; Cornell University Press: Ithaca, NY, 1979. (b) de Gennes, P. G. *J. Chem. Phys.* **1980**, *72*, 4756.

(7) Pincus, P. *J. Chem. Phys.* **1981**, *75*, 1996.

(8) Binder, K. *J. Chem. Phys.* **1983**, *79*, 6387.

(9) Flory, P. J. *Principles of Polymer Chemistry*; Cornell University Press: Ithaca, NY, 1953.

(10) (a) Jones, R. A. L.; Norton, L.; Kramer, E. J.; Bates, F. S.; Wiltzius, P. *Phys. Rev. Lett.* **1991**, *66*, 1326. (b) Wiltzius, P.; Cumming, A. *Phys. Rev. Lett.* **1991**, *66*, 3000. (c) Wiltzius, P.; Cumming, A.; Bates, F. S.; Rosedale, J. H. *Phys. Rev. A* **1992**, *45*, 885. (d) Bruder, F.; Brenn, R. *Phys. Rev. Lett.* **1992**, *69*, 624. (e) Krausch, G.; Dai, C.-A.; Kramer, E. J.; Marko, J. F.; Bates, F. S. *Macromolecules* **1993**, *26*, 5566. (f) Geoghegan, M.; Ermer, H.; Jüngst, G.; Krausch, G.; Brenn, R. *Phys. Rev. E* **2000**, *62*, 940. (g) Sung, L.; Karim, A.; Douglas, J. F.; Han, C. C. *Phys. Rev. Lett.* **1996**, *76*, 4368. (h) Nakai, A.; Shiwaku, T.; Wang, W.; Hasegawa, H.; Hashimoto, T. *Macromolecules* **1996**, *29*, 5990. (i) Wang, W.; Shiwaku, T.; Hashimoto, T. *Macromolecules* **2003**, *36*, 8088. (j) Wang, H.; Composto, R. J. *Phys. Rev. E* **2000**, *61*, 1659. (k) Xie, X.-M.; Chen, Y.; Zhang, Z.-M.; Tanioka, A.; Matsuoka, M.; Takemura, K. *Macromolecules* **1999**, *32*, 4424. (m) Krausch, G.; Dai, C.-A.; Kramer, E. J.; Bates, F. S. *Phys. Rev. Lett.* **1993**, *71*, 3669.

(11) (a) Puri, S.; Binder, K. *Phys. Rev. A* **1992**, *46*, R4487. (b) Puri, S.; Binder, K. *Phys. Rev. E* **1994**, *49*, 5359. (c) Puri, S.; Binder, K. *Phys. Rev. E* **1997**, *56*, 6991. (d) Puri, S.; Binder, K. *Phys. Rev. Lett.* **2001**, *86*, 1797. (e) Puri, S.; Binder, K. *Phys. Rev. E* **2002**, *66*, 061602. (f) Marko, J. F. *Phys. Rev. E* **1993**, *48*, 2861. (g) Toxvaerd, S. *Phys. Rev. Lett.* **1999**, *83*, 5318. (h) Rysz, J. *Polymer* **2005**, *46*, 977. (i) Yan, L.-T.; Xie, X.-M. *Polymer* **2005**, *46*, 7684. (j) Yan, L.-T.; Xie, X.-M. *Macromol. Theory Simul.*, in press. (k) Chen, H.; Chakrabarti, A. *Phys. Rev. E* **1997**, *55*, 5680. (l) Binder, K.; Landau, D.; Müller, M. *J. Stat. Phys.* **2003**, *110*, 1411.

(12) For reviews of experimental studies of this problem, see: Geoghegan, M.; Krausch, G. *Prog. Polym. Sci.* **2003**, *28*, 261. For reviews of numerical simulations of this problem, see: Puri, S.; Frisch, H. L. *J. Phys.: Condens. Matter* **1997**, *9*, 2109. Puri, S. *J. Phys.: Condens. Matter* **2005**, *17*, R101.

(13) Jiang, Z.; Ebner, C. *Phys. Rev. B* **1989**, *39*, 2501.

(14) (a) San Miguel, M.; Grant, M.; Gunton, J. D. *Phys. Rev. A* **1985**, *31*, 1001. (b) Grant, M.; Elder, K. R. *Phys. Rev. Lett.* **1999**, *82*, 14.

(15) Cook, H. E. *Acta Metall.* **1970**, *18*, 297.

(16) Genzer, J.; Composto, J. *Europhys. Lett.* **1997**, *38*, 171.

(17) Schmidt, I.; Binder, K. *J. Phys. (Paris)* **1985**, *46*, 1631.

(18) (a) Kawasaki, K. In *Phase Transitions and Critical Phenomena*; Domb, C., Green, M. S., Eds.; Academic: London, 1972; Vol. 2; Chapter 11. (b) Binder, K.; Frisch, H. L. *J. Phys. B* **1991**, *84*, 403.

(19) (a) Clarke, N. *Phys. Rev. Lett.* **2002**, *89*, 215506. (b) Henderson, I. C.; Clarke, N. *Macromolecules* **2004**, *37*, 1952. (c) Henderson, I. C.; Clarke, N. *Macromol. Theory Simul.* **2005**, *14*, 435.

(20) Glotzer, S. C. *Annu. Rev. Comput. Phys.* **1995**, *2*, 1.

(21) (a) Oono, Y.; Puri, S. *Phys. Rev. A* **1988**, *38*, 434. (b) Puri, S.; Oono, Y. *Phys. Rev. A* **1988**, *38*, 1542.

(22) Ohta, T.; Enomoto, Y.; Harden, J. L.; Doi, M. *Macromolecules* **1993**, *26*, 4928.

(23) It should be noted that the form of μ_b used here is based on the ϕ^4 free energy function.[11d,e] Although it is not the Flory−Huggins−de Gennes free energy used in this simulation, it is still reasonable because, physically, the model used in the simulation should have applicability when other forms of the free energy are used.[19c]

(24) Brown, G.; Chacrabarti, A. *Phys. Rev. A* **1992**, *46*, 4829.

MA0524878